Clinical Chemistry 63:5
1008–1021 (2017)

Distinguishing Intake of New Synthetic Cannabinoids ADB-PINACA and 5F-ADB-PINACA with Human Hepatocyte Metabolites and High-Resolution Mass Spectrometry

Jeremy Carlier,[1] Xingxing Diao,[1,2] Karl B. Scheidweiler,[1] and Marilyn A. Huestis[1,3*]

BACKGROUND: ADB-PINACA and its 5-fluoropentyl analog 5F-ADB-PINACA are among the most potent synthetic cannabinoids tested to date, with several severe intoxication cases. ADB-PINACA and 5F-ADB-PINACA have a different legal status, depending on the country. Synthetic cannabinoid metabolites predominate in urine, making detection of specific metabolites the most reliable way for proving intake in clinical and forensic specimens. However, there are currently no data on ADB-PINACA and 5F-PINACA metabolism. The substitution of a single fluorine atom distinguishes the 2 molecules, which may share common major metabolites. For some legal applications, distinguishing between ADB-PINACA and 5F-PINACA intake is critical. For this reason, we determined the human metabolic fate of the 2 analogs.

METHODS: ADB-PINACA and 5F-PINACA were incubated for 3 h with pooled cryopreserved human hepatocytes, followed by liquid chromatography—high-resolution mass spectrometry analysis. Data were processed with Compound Discoverer.

RESULTS: We identified 19 and 12 major ADB-PINACA and 5F-ADB-PINACA metabolites, respectively. Major metabolic reactions included pentyl hydroxylation, hydroxylation followed by oxidation (ketone formation), and glucuronidation of ADB-PINACA, and oxidative defluorination followed by carboxylation of 5F-ADB-PINACA.

CONCLUSIONS: We recommend ADB-PINACA ketopentyl and hydroxypentyl, and ADB-PINACA 5-hydroxypentyl and pentanoic acid, as optimal markers for ADB-PINACA and 5F-ADB-PINACA intake, respectively. Since the 2 compounds present positional isomers as the primary metabolites, monitoring unique product ions and optimized chromatographic conditions are required for a clear distinction between ADB-PINACA and 5F-ADB-PINACA intake.

Synthetic cannabinoids (SC)[4] are novel psychoactive substances designed to stimulate the endocannabinoid system and mimic the effects of Δ^9-tetrahydrocannabinol, the main psychoactive constituent of cannabis *(1)*. Although originally developed as research tools, the consumption of SC as "legal highs" gained wide popularity in 2008 *(2)*, producing dangerous behaviors, severe intoxications, and fatalities *(3, 4)*, leading many countries to schedule them as illicit drugs. However, new substances are constantly replacing newly controlled drugs, and legislative authorities struggle to keep up with the dynamic market *(5, 6)*.

ADB-PINACA [*N*-(1-amino-3,3-dimethyl-1-oxo-2-butanyl)-1-pentyl-1*H*-indazole-3-carboxamide] and its 5-fluoropentyl derivative 5F-ADB-PINACA (*N*-[(2S)-1-amino-3,3-dimethyl-1-oxo-2-butanyl]-1-(5-fluoropentyl)-1*H*-indazole-3-carboxamide) were first mentioned in online drug forums in 2013 *(7)*, making them 2 of the newest SC. The 2 compounds were designed to maximize potency, with an indazole core substituted at C_3 by a 3,3-dimethylbutanamide side-chain via a carboxamide link, and on N_1 by a pentyl or 5-fluoro-pentyl tail (Fig. 1). ADB-PINACA and 5F-ADB-PINACA median effective concentration (EC_{50}) = 0.52 and 0.24 nmol/L, respectively, for the activation of central cannabinoid receptors 1, and EC_{50} = 0.88 and 2.6 nmol/L for the

[1] Chemistry & Drug Metabolism Section, Clinical Pharmacology & Therapeutics Research Branch, Intramural Research Program, National Institute on Drug Abuse, National Institutes of Health, Baltimore, MD; [2] Current address: XenoBiotic Laboratories, Inc., 107 Morgan Lane, Plainsboro, NJ; [3] School of Medicine, University of Maryland, Baltimore, MD.
* Address correspondence to this author at: University of Maryland School of Medicine, 683 Shore Rd., Severna Park, MD 21146. Fax 410-544-2456; e-mail marilyn.huestis@gmail.com.

Received September 30, 2016; accepted December 21, 2016.
Previously published online at DOI: 10.1373/clinchem.2016.267575

[4] Nonstandard abbreviations: SC, synthetic cannabinoid; EC_{50}, median effective concentration; FullMS/ddMS^2, full-scan MS/data-dependent MS/MS acquisition mode; AGC, automatic gain control; IT, injection time; FullMS/AIF/ddMS^2, full-scan MS/all-ion fragmentation/data-dependent MS/MS acquisition mode.

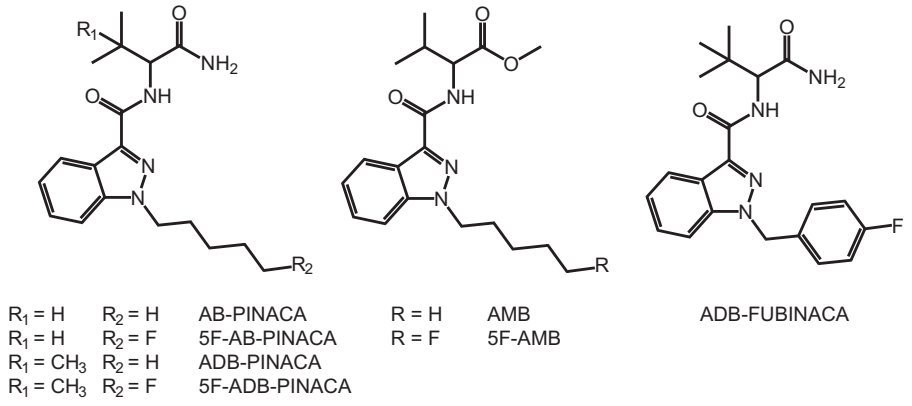

Fig. 1. Structure of ADB-PINACA, 5F-ADB-PINACA, and analogs.

activation of peripheral cannabinoid receptors 2. These SC are 330 and 715 times more potent at cannabinoid receptor type 1 than Δ^9-tetrahydrocannabinol, respectively (among the most potent SC reported to date) *(8)*.

In late 2013, an outbreak of ADB-PINACA exposure associated with neurotoxicity and cardiotoxicity occurred in Colorado *(9)* and Georgia *(10)* (US). Patients were delusional, agitated, and anxious/aggressive, presenting with tachycardia and high blood pressure. A case of cardiac arrest was reported, although the patient had a medical history of familial artery disease and cocaine use. Generalized seizures were reported up to 7 days after intake *(10)*. Following this intoxication series and ADB-PINACA seizures in the UK in 2013, the European Monitoring Centre for Drugs and Drug Addiction issued an alert in 2014 *(11)*. In 2013, approximately 260 cases of possible exposure were reported in less than 1 month in Europe *(12)*. 5F-ADB-PINACA was first identified in herbal products in Japan *(13)* and in Europe as a result of seizures in 2015 in Sweden *(14)*. No intoxication cases related to 5F-ADB-PINACA have been identified to date, despite its high potency *(8)*. ADB-PINACA was scheduled in the US in 2014 *(15, 16)* and in China in 2015 *(17)*. Both compounds are controlled in Japan *(18)* and Singapore *(19)*. Because of different legal status in different countries, differentiating ADB-PINACA and 5F-ADB-PINACA intake is critical.

Urine is the matrix of choice for providing evidence of intake in clinical and forensic cases. Because the window of detection in urine is generally much longer than for blood or oral fluid, sufficient sample can be noninvasively collected, and metabolites are concentrated for several days after intake. Due to their high potencies, many SC are active at low doses and are extensively metabolized *(20–22)*. Consequently, the parent SC is usually not found in urine, making metabolites detection critical for documenting intake. In several cases of ADB-PINACA intoxication, the parent SC was detected in serum or plasma the day of intake only (50–307 and 50–65 μg/L, respectively), although its metabolite, ADB-PINACA pentanoic acid, was detected up to 3 days after intake and symptoms of intoxication persisted up to 7 days after intake *(10)*. However, ADB-PINACA pentanoic acid is the only ADB-PINACA metabolite reported to date *(10)*, and ADB-PINACA and 5F-ADB-PINACA metabolism is yet to be elucidated. SC and 5-fluoro analogs do not always display a similar pattern of major urinary metabolites and, conversely, may share common metabolites, making it challenging to distinguish their intake *(23–25)*.

We aimed to investigate ADB-PINACA and 5F-ADB-PINACA human metabolism to identify major specific urinary markers for intake. Since controlled administration of novel psychoactive substances in humans is fraught with the lack of in vitro and preclinical toxicity data, we used in vitro incubation of certified standards with human hepatocytes, which proved successful in predicting the human urinary marker metabolites of many SC *(23–29)*. Human hepatocytes contain all hepatic metabolic enzymes and cofactors in similar conditions to in vivo, providing better prediction of optimal metabolites in humans than purified enzymes or human liver microsomes *(30)*. We analyzed incubations with liquid chromatography–high resolution tandem mass spectrometry, according to our standardized protocol for metabolite identification *(23–29)*.

Methods

CHEMICALS AND REAGENTS

ADB-PINACA and 5F-ADB-PINACA standards were purchased from Cayman Chemical and dissolved in methanol. LC-MS grade water, methanol, and formic acid (Optima™ LC/MS) were acquired from Fisher Scientific, and LC-MS grade acetonitrile from Sigma-Aldrich®.

HEPATOCYTE INCUBATION AND SAMPLE PREPARATION

Hepatocyte incubation and sample preparation were consistent with our protocol, as previously described *(23–29)* and as detailed in the Supplemental Hepatocyte and Sample Preparation file that accompanies the online version of this article at http://www.clinchem.org/content/vol63/issue5.

Briefly, 250 μL of 10 μmol/L ADB-PINACA or 5F-ADB-PINACA in KHB (BioreclamationIVT) was incubated at 37 °C for 3 h with 250 μL 2×10^6 cells/mL cryopreserved hepatocytes (BioreclamationIVT). The reaction was quenched with 500 μL acetonitrile and samples were stored at −80 °C until analysis.

Samples were thawed; 100 μL was mixed with 100 μL acetonitrile and centrifuged at 4 °C for 10 min at 15000*g*. Supernatants were evaporated to dryness and reconstituted in 150 μL mobile phase A:B 80:20 (v/v). Fifteen microliters were injected onto the chromatographic system.

LIQUID CHROMATOGRAPHY-HIGH-RESOLUTION TANDEM MASS SPECTROMETRY PARAMETERS

Liquid chromatography–high-resolution tandem mass spectrometry analysis was performed on a Q Exactive™ Plus mass spectrometer equipped with a heated electrospray operating in positive-ion mode (Thermo Scientific) and coupled with an Ultimate™ 3000 LC system from Dionex. Data were acquired with Xcalibur software (Thermo Scientific).

Separation was performed on an Ultra Biphenyl column (100 × 2.1 mm, 3 μm) from Restek®, combined with an identically packed guard cartridge (10 × 2.1 mm). Elution was achieved within 15 min with a gradient mobile phase composed of 0.1% formic acid in water (A) and 0.1% formic acid in acetonitrile (B) at a flow rate of 0.5 mL/min. The gradient started with 20% B for 0.5 min, was ramped to 95% B at 11 min, held for 2 min, returned to initial conditions within 0.1 min, and was reequilibrated for 1.9 min. Autosampler and column oven temperatures were 4 and 30 °C, respectively.

Ionization source parameters and collision energies were optimized on the parent signal by postcolumn infusion of ADB-PINACA and 5F-ADB-PINACA standards in A:B 50:50 (v/v) at 0.5 mL/min. Source parameters were: spray voltage, 4 kV; sheath gas flow rate, 40 arbitrary units (a.u.); auxiliary gas flow rate, 5 a.u.; sweep gas flow rate, 2 a.u.; S-lens radio frequency level, 50 a.u.; auxiliary gas heater temperature, 400 °C; capillary temperature, 300 °C.

On a first injection, data were acquired in full-scan MS/data-dependent MS/MS mode (FullMS/ddMS^2). MS cycles were composed of 1 FullMS and up to 5 ddMS^2 (*m/z*-1.5 isolation window) scans. The 5 ions with the most intense signal detected in the full MS survey scan (intensity threshold, 2.0×10^4) triggered a specific MS/MS spectrum. An inclusion list was added to prioritize the fragmentation of expected metabolites based on the literature *(23–25, 29)* (see online Supplemental Table 1). Full MS settings were: resolution (full width at half maximum at *m/z* 200), 70 000; scan range, *m/z* 150–650; automatic gain control (AGC) target, 1.0×10^6; and maximum injection time (IT), 200 ms. ddMS^2 settings were: resolution, 17 500; AGC target, 1.0×10^5; maximum IT, 50 ms; stepped collision energy, 30 (20)%; apex triggering, 3–6 s; and dynamic exclusion, 2 s.

On a second injection, data were acquired in full-scan MS/all-ion fragmentation/data-dependent MS/MS mode (FullMS/AIF/ddMS^2). MS cycles were composed of 1 FullMS, 1 AIF (*m/z* 150–650 isolation window) and up to 5 ddMS^2 scans. The 5 ions with the most intense signal detected in the full MS survey scan (intensity threshold, 2.0×10^4) and in the AIF survey scan with specific neutral losses, triggered a specific MS/MS spectrum. The list of neutral losses was based on ADB-PINACA and 5F-ADB-PINACA fragmentation pattern; sulfate and glucuronide losses were included to identify phase II metabolites (see online Supplemental Table 1). FullMS and ddMS2 settings were the same as described above. AIF settings were: resolution, 17 500; AGC target, 1.0×10^5; maximum IT, 50 ms; and stepped collision energy, 30 (20)%. Results from the 2 acquisition modes were compared in online Supplemental Comparison of Two Acquisition Modes file.

METABOLITE IDENTIFICATION

Raw data from incubations with both acquisition modes were processed with Compound Discoverer™ (Thermo Scientific). A list of potential metabolites was generated and biotransformations were suggested for each chromatographic peak depending on the mass and the isotopic pattern of the corresponding compound. Mass tolerance for MS identification was 5 ppm, minimum MS peak intensity was 0.1% of the metabolite with the most intense signal (3.6×10^3 and 1.0×10^4 for ADB-PINACA and 5F-ADB-PINACA, respectively), and intensity tolerance for the isotope search was 50%; settings for compound generation are described in online Supplemental Table 2.

Results and Discussion

ADB-PINACA AND 5F-ADB-PINACA FRAGMENTATION

ADB-PINACA eluted at 6.57 min ($[M+H]^+$, *m/z* 345.2281) and yielded characteristic fragments by neutral loss of amine (*m/z* 328.2014), carboxamide (*m/z* 300.2065), dimethylbutanamide (*m/z* 233.1283), or aminodimethylbutanamide (*m/z* 215.1176) groups. Further *N*-alkyl chain loss from fragments *m/z* 215.1176 and 233.1283 produced ions *m/z* 145.0394 and 163.0500, respectively (Fig. 2).

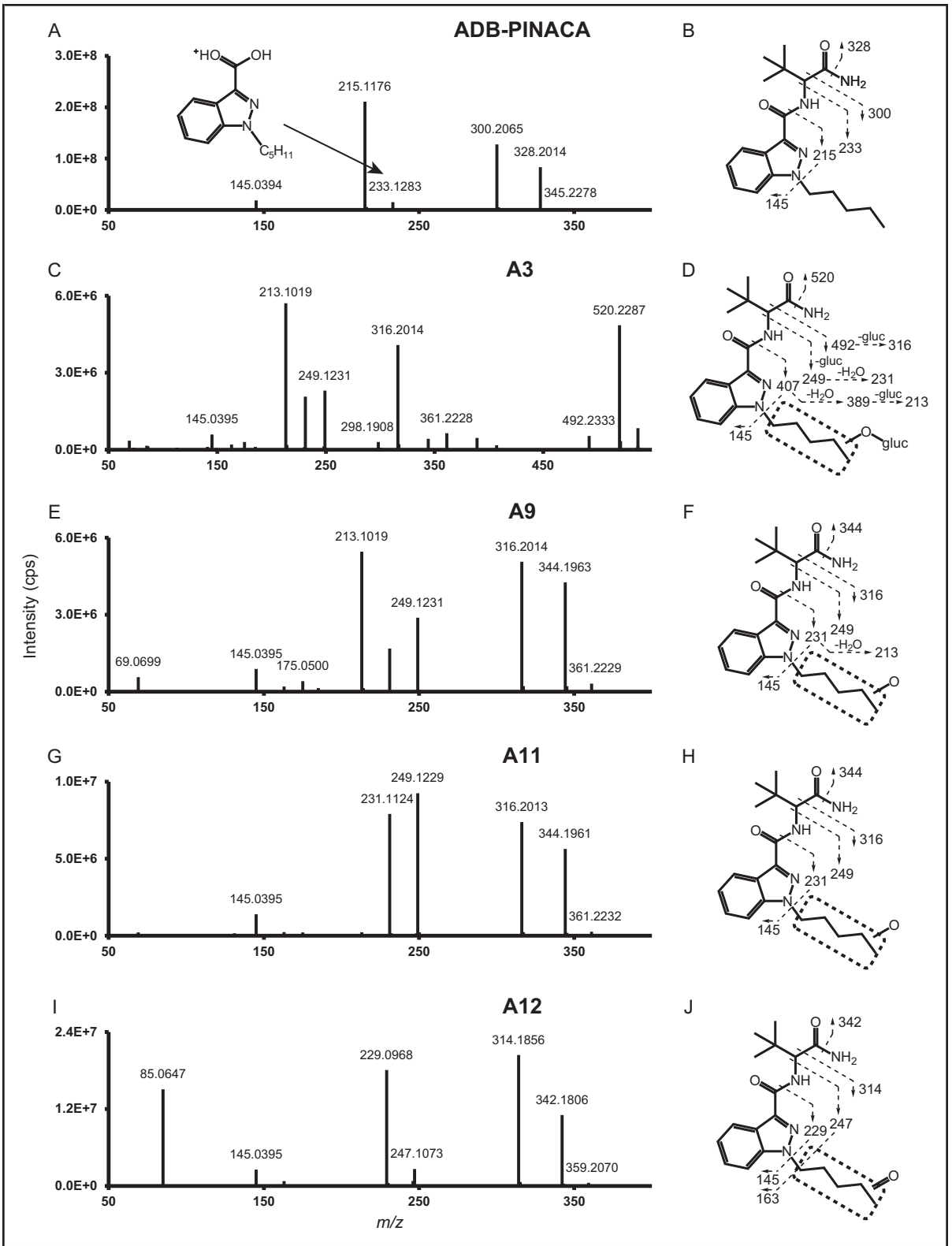

Fig. 2. ADB-PINACA, A3, A9, A11, and A12's MS/MS spectra (A, C, E, G, and I, respectively) and assigned fragmentation pattern (B, D, F, H, and J, respectively) (major metabolites).

5F-ADB-PINACA eluted earlier, at 5.98 min ($[M+H]^+$, *m/z* 363.2190), and displayed a similar MS/MS pattern. Major fragments were formed by loss of amine (*m/z* 346.1919), carboxamide (*m/z* 318.1970), dimethylbutanamide (*m/z* 251.1187), or aminodimethylbutanamide (*m/z* 233.1081); fragments *m/z* 145.0394 and 163.0499, also were present. In addition, fragment *m/z* 213.1081 was produced by further hydrofluoric acid loss from fragment *m/z* 233.1081 and ion *m/z* 177.0455 was possibly formed by fluorine rearrangement, as previously reported (Fig. 3) *(28)*.

ADB-PINACA METABOLITES IN HUMAN HEPATOCYTES

ADB-PINACA chromatographic peak area decreased to 11% after 3-h incubation with human hepatocytes. Thirty-five metabolites were identified, with >95% of the metabolites' total peak area represented by 19 metabolites (described below A1–A19 in ascending retention time order, Fig. 4). Results are compiled in Table 1. MS/MS spectra and fragmentation patterns are depicted in Fig. 2, with the data for 15 minor metabolites provided in the online Supplemental Figs. 1–3. A proposed metabolic pathway for ADB-PINACA is described in Fig. 4. The dominant phase I reactions were hydroxylations and hydroxylation followed by oxidation at the pentyl chain (A1, A2, A8, A9, A11–A14; A3, as glucuronide) or the indazole ring (A15; A5, A6 as glucuronides). These transformations are common in the metabolism of structural analogs *(23–25, 29)*. Minor reactions included isopropyl chain hydroxylation (A8, A16, A17), pentyl carboxylation (A10), oxidative deamination of the carboxamide group (A18, A19), dehydrogenation (A16, A19), *N*-depentylation (A4), and epoxidation followed by hydrolysis (A7). Phase II glucuronidation occurred in 3 of 19 metabolites (A3, A5, and A6). A12 (ketopentyl), A11 (hydroxypentyl), and A9 (hydroxypentyl) were the metabolites with the most intense signal, respectively, totaling 49% of metabolites' total peak area.

ADB-PINACA OXIDATION AND FURTHER GLUCURONIDATION, KETONE FORMATION, DEHYDROGENATION, OR CARBOXYLATION

A9, A11, and A13 were the result of ADB-PINACA hydroxylation (+O) as indicated by the +15.9950-Da mass shift from parent. The mass difference was observed with all fragments, except for *m/z* 145.0395 and 163.0499, suggesting a hydroxylation at the pentyl chain. *m/z* 213.1019 was produced by aminodimethylbutanamide and water losses; remarkably, this fragment had the most intense signal in the A9 MS/MS spectrum, although it was almost absent from A11 and A13 spectra, in which ions *m/z* 249.1229 and 231.1125, respectively, were dominating. The investigation of 5F-ADB-PINACA metabolism, in which ADB-PINACA 5-hydroxypentyl was detected (F7), indicates that A9, A11, and A13 site of attack was not C_5. Similarly, A15 presented a +15.9951-Da shift from parent. All fragments presented the same mass difference, including fragments *m/z* 161.0344 and 179.0451 (*m/z* 145.0394 and 163.0500 +O, respectively), indicating a hydroxylation at the indazole moiety. A17 also was formed by hydroxylation, as indicated by the +15.9950-Da shift from ADB-PINACA. However, its MS/MS spectrum presented the same fragments as parent, except for *m/z* 344.1962 and 316.2013, respectively produced by amine and carboxamide loss, indicating a hydroxylation at the isopropyl chain. Interestingly, fragment *m/z* 316.2013 displayed a low signal intensity in favor of *m/z* 286.1909, produced by subsequent hydroxymethyl loss, as observed in the fragmentation of ADB-FUBINACA metabolites with the same biotransformation *(29)*.

Pentyl hydroxylation and following glucuronidation ($+C_6H_8O_6$) occurred in A3, whose signal was included in a characteristic cluster and had a +192.0276-Da mass deviation from parent (+15.9949 +176.0327 Da). Detection of A9, A11, and A13 fragments, along with amine, carboxamide, and aminodimethylbutanamide losses, in the A3 MS/MS spectrum indicates a hydroxyglucuronidation at the pentyl chain. Fragments' relative intensity suggests that A3 was produced by glucuronidation of A9, rather than A11 or A13. Following the same reasoning, A6 was identified as A15 glucuronide.

Oxidation occurred in A12 and A14, resulting in a ketone formation (+O –2H). Mechanism of formation was a hydroxylation followed by oxidation rather than a one-step formation, as suggested by the detection of hydroxylated metabolites. Precursor and fragments' mass shift from ADB-PINACA (+15.9949 −2.0154 Da), apart from fragments *m/z* 145.0395 and 163.0499, indicates ketone formation at the pentyl chain. Although the MS/MS spectrum does not allow precise location of the ketone on the pentyl sidechain, the reaction probably occurred at the C_4 and C_1 in A12 and A14, respectively, as suggested by the metabolism of other compounds with an aliphatic side chain *(31, 32)*. A16 presented the same mass shift from parent (+13.9794 Da), but this shift was only transferred to the fragment produced by the amine loss, indicating a hydroxylation and a dehydrogenation at the isopropyl chain. In this case, imine formation is more stable and is, therefore, more likely than ketone formation.

Carboxylation at the pentyl chain also was observed in A10 at a low intensity. The fragmentation spectrum displayed the 3 major characteristic ions *m/z* 217.0969, 245.0917, and 227.0811, respectively produced by formamidodimethylbutanamide loss and aminodimethylbutanamide and subsequent water losses, as previously observed in structural analogs *(24, 25)*. Subsequent carboxylic acid loss from *m/z* 245.0917–199.0864 further confirmed the carboxylation. Although it had a low sig-

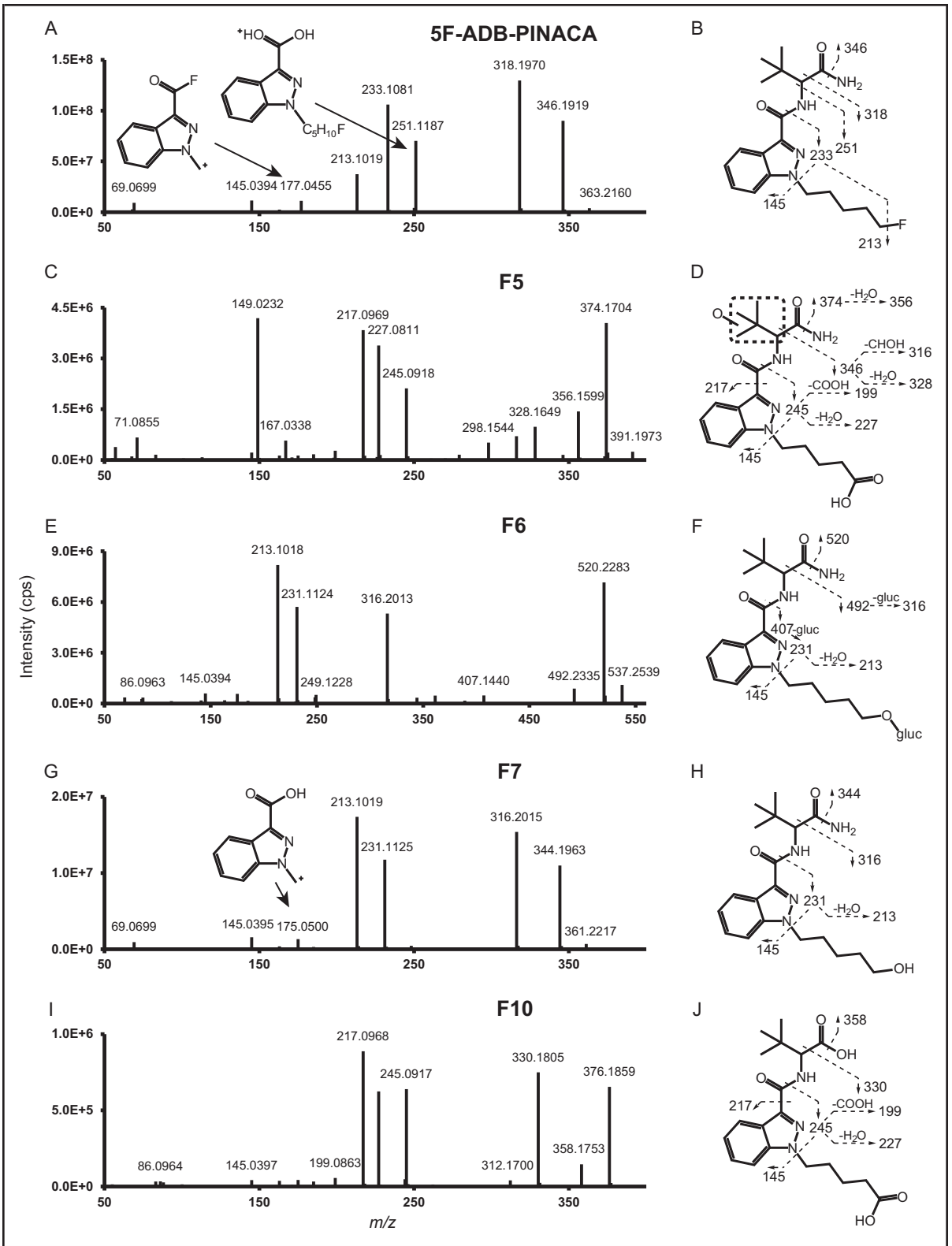

Fig. 3. 5F- ADB-PINACA, F5, F6, F7, and F10's MS/MS spectra (A, C, E, G, and I, respectively) and assigned fragmentation pattern (B, D, F, H, and J, respectively) (major metabolites).

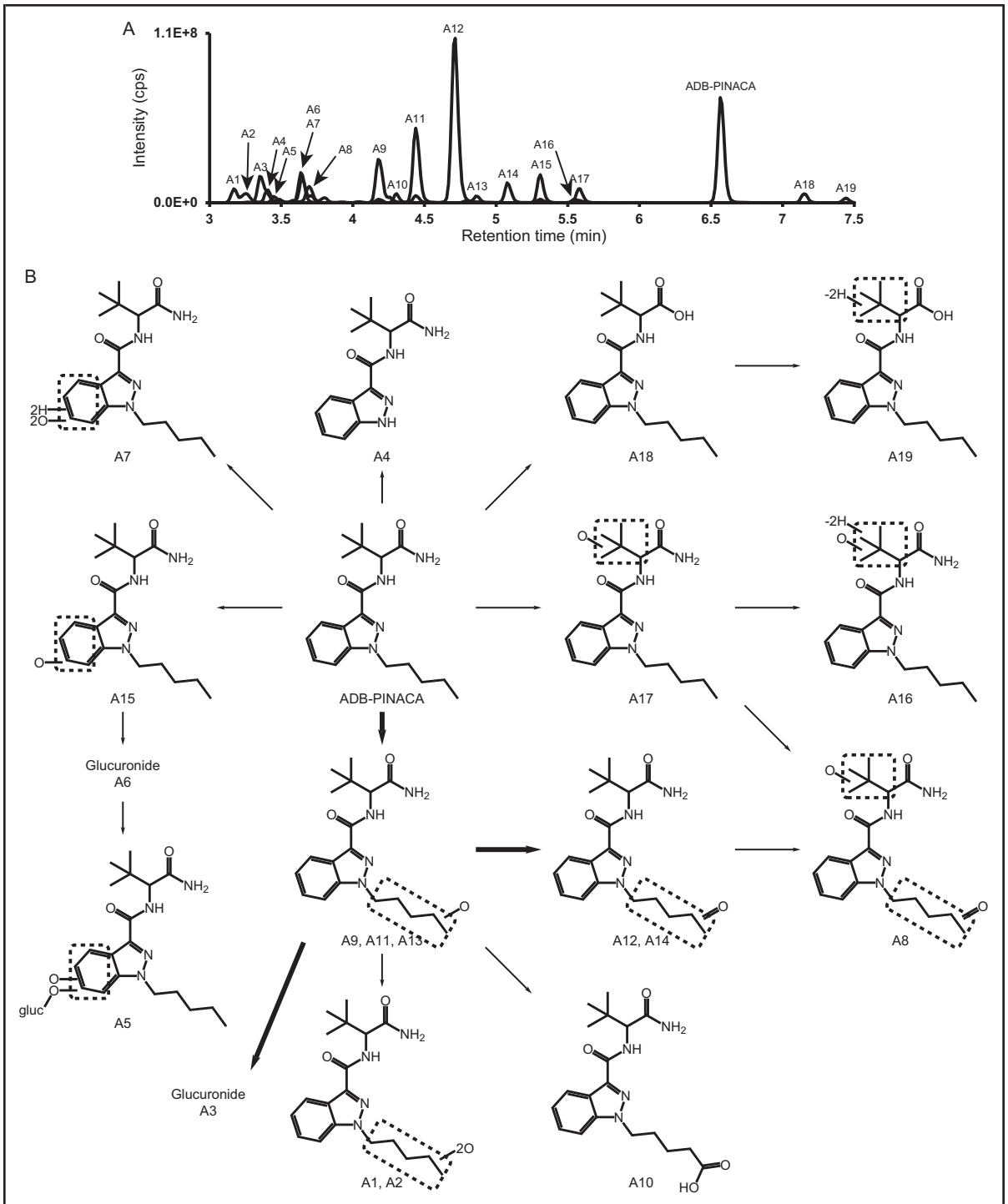

Fig. 4. Combined extracted ion chromatogram (A) and proposed metabolic pathway (B) of ADB-PINACA and metabolites obtained from 3-h hepatocyte incubation.

Bold arrow, major pathway; gluc, glucuronide.

Table 1. Accurate mass molecular ion, retention time, elemental composition, nominal mass for diagnostic product ions, mass spectrometry peak areas, and ADB-PINACA and 5F-ADB-PINACA metabolite peak area fraction (sum = 95.4 and 95.2%, respectively) in hepatocyte incubations.[a]

ID	Biotransformation	$[M+H]^+$, *m/z*	Retention time, min	Mass error, ppm	Elemental composition	Diagnostic product ions, *m/z*	Peak area at $T_{3\,h}$	Metabolites peak area fraction, %
	ADB-PINACA	345.2281	6.57	0.85	C19H28N4O2	145, 215, 233, 300, 328	2.8×10^6	
A1	Dihydroxylation (pentyl chain)	377.2182	3.18	0.43	C19H28N4O4	145, 247, 265, 332, 360	2.9×10^5	2.1
A2	Dihydroxylation (pentyl chain)	377.2182	3.25	0.43	C19H28N4O4	145, 213, 265, 332, 360	2.2×10^5	1.6
A3	Hydroxylation (pentyl chain) + glucuronidation	537.2557	3.36	−0.32	C25H36N4O9	213, 231, 249, 316, 520	1.1×10^6	7.7
A4[b]	*N*-Dealkylation (pentyl chain)	275.1501	3.41	0.61	C14H18N4O2	145, 163, 230, 258	3.0×10^5	2.2
A5	Dihydroxylation (indazole ring) + glucuronidation	553.2507	3.45	−0.45	C25H36N4O10	247, 265, 423, 441, 536	1.9×10^5	1.4
A6	Hydroxylation (indazole ring) + glucuronidation	537.2558	3.64	−0.55	C25H36N4O9	161, 231, 407, 492, 520	9.0×10^5	6.6
A7	Dihydrodiol formation (indazole ring)	379.2338	3.64	0.49	C19H30N4O4	179, 249, 267, 334, 362	8.3×10^5	6.1
A8	Ketone formation (pentyl chain) + hydroxylation (isopropyl chain)	375.2026	3.70	0.30	C19H26N4O4	145, 229, 300, 330, 358	2.2×10^5	1.6
A9	Hydroxylation (pentyl chain)	361.2231	4.18	0.84	C19H28N4O3	213, 231, 249, 316, 344	1.2×10^6	8.4
A10[c]	Carboxylation (pentyl chain)	375.2025	4.30	0.53	C19H26N4O4	217, 227, 245, 330, 358	2.4×10^5	1.8
A11	Hydroxylation (pentyl chain)	361.2230	4.44	1.26	C19H28N4O3	145, 231, 249, 316, 344	1.8×10^6	13.3
A12	Ketone formation (pentyl chain)	359.2075	4.71	0.86	C19H26N4O3	145, 229, 247, 314, 342	3.7×10^6	26.8
A13	Hydroxylation (pentyl chain)	361.2231	4.87	0.76	C19H28N4O3	145, 231, 249, 316, 344	1.7×10^5	1.3
A14	Ketone formation (pentyl chain)	359.2076	5.08	0.36	C19H26N4O3	145, 229, 247, 314, 342	3.1×10^5	2.2
A15	Hydroxylation (indazole ring)	361.2232	5.31	0.67	C19H28N4O3	161, 231, 249, 316, 344	7.8×10^5	5.7
A16	Hydroxylation (isopropyl chain) + dehydrogenation (isopropyl chain)	359.2075	5.55	0.77	C19H26N4O3	145, 215, 233, 341	1.0×10^5	0.8
A17	Hydroxylation (isopropyl chain)	361.2231	5.58	1.01	C19H28N4O3	145, 215, 233, 286, 344	4.0×10^5	2.9
A18	Oxidative deamination	346.2123	7.15	0.51	C19H27N3O3	145, 215, 233, 300, 328	3.2×10^5	2.3
A19	Oxidative deamination + dehydrogenation (isopropyl chain)	344.1968	7.44	0.26	C19H25N3O3	145, 163, 215, 233, 286	1.1×10^5	0.8

Continued on page 1016

Table 1. Accurate mass molecular ion, retention time, elemental composition, nominal mass for diagnostic product ions, mass spectrometry peak areas, and ADB-PINACA and 5F-ADB-PINACA metabolite peak area fraction (sum = 95.4 and 95.2%, respectively) in hepatocyte incubations. *(Continued from page 1015)*

ID	Biotransformation	$[M+H]^+$, *m/z*	Retention time, min	Mass error, ppm	Elemental composition	Diagnostic product ions, *m/z*	Peak area at $T_{3\,h}$	Metabolites peak area fraction, %
	5F-ADB-PINACA	363.2190	5.98	0.32	C19H27FN4O2	213, 233, 251, 318, 346	5.3×10^3	
F1	OD[d] + hydroxylation (pentyl chain)	377.2180	3.14	0.75	C19H28N4O4	175, 229, 247, 332, 360	3.9×10^5	1.8
F2	Hydroxylation (indazole ring) + glucuronidation	555.2458	3.31	0.42	C25H35FN4O9	229, 249, 267, 443, 538	2.7×10^5	1.2
F3	OD + hydroxylation (isopropyl chain)	377.2181	3.39	0.59	C19H28N4O4	145, 213, 231, 302, 360	4.6×10^5	2.1
F4	*N*-dealkylation	275.1502	3.41	0.27	C14H18N4O2	145, 163, 230, 258	5.0×10^5	2.3
F5	OD + oxidation to carboxylic acid + hydroxylation (isopropyl chain)	391.1973	3.43	0.85	C19H26N4O5	217, 227, 245, 356, 374	9.6×10^5	4.4
F6	OD + glucuronidation	537.2553	3.49	0.36	C25H36N4O9	213, 231, 316, 492, 520	9.5×10^5	4.3
F7	OD	361.2231	4.28	0.92	C19H28N4O3	145, 213, 231, 316, 344	3.0×10^6	13.5
F8	Hydroxylation (pentyl chain)	379.2134	4.30	1.55	C19H27FN4O3	145, 249, 267, 334, 362	2.7×10^5	1.2
F9	OD + oxidation to carboxylic acid	375.2023	4.32	1.10	C19H26N4O4	217, 227, 245, 330, 358	1.3×10^7	61.3
F10	OD + oxidation to carboxylic acid + oxidative deamination	376.1864	4.91	0.87	C19H25N3O5	217, 227, 245, 330, 358	1.4×10^5	0.7
F11	OD + oxidative deamination + dehydrogenation (isopropyl chain)	360.1914	4.99	0.96	C19H25N3O4	145, 175, 213, 231, 342	1.7×10^5	0.8
F12	OD + oxidation to carboxylic acid + oxidative deamination + dehydrogenation (isopropyl chain)	374.1708	5.02	0.56	C19H23N3O5	217, 227, 245, 328, 356	3.5×10^5	1.6

[a] Peak area for ADB-PINACA and 5F-ADB-PINACA at $T_{0\,h}$ was 2.6×10^7 and 3.1×10^7, respectively. Metabolites are listed by ascending retention time.
[b] A4 = F4.
[c] A10 = F9.
[d] OD, oxidative defluorination.

nal intensity in our hepatocyte incubations, ADB-PINACA pentanoic acid was detected in serum and plasma of several cases of intoxication up to 3 days following ADB-PINACA intake *(10)*.

A1, A2, A5, and A8 were minor second or third generation metabolites combining hydroxylation, ketone formation, and glucuronidation, identified as described above, with A1 and A2 dihydroxypentyl metabolites, and A5 and A8 dihydroxyindazole-glucuronide and hydroxy-isopropyl-ketopentyl metabolites, respectively.

ADB-PINACA OXIDATIVE DEAMINATION AND FURTHER DEHYDROGENATION

Another common reaction in structural analogs metabolism is the oxidative deamination of the carboxamide group, resulting in a carboxylic acid function *(23, 27, 29)*. A18 was produced by ADB-PINACA oxidative deamination, which presented as a +0.9842-Da shift ($-NH_2$ +OH) and the same fragments as the parent. A18 was not a major metabolite as opposed to AB-PINACA *(23)*, AB-FUBINACA *(27)*, and ADB-FUBINACA *(29)* metabolism. This phenomenon is easy to understand for AB- and ADB-FUBINACA since these compounds do not carry a pentyl chain that is the primary site of attack for AB-PINACA and ADB-PINACA. In the case of AB-PINACA, the desmethyl isomer of ADB-PINACA, replacement of the isopropyl by a *tert*-butyl group may favor the action of the metabolic enzyme at the carboxamide. As a matter of fact, amide hydrolysis is more important in AB-FUBINACA (*tert*-butyl) than ADB-FUBINACA (isopropyl) metabolism. A19 was produced by subsequent A18 dehydrogenation at the isopropyl group, as discussed above.

ADB-PINACA *N*-DEPENTYLATION

ADB-PINACA *N*-dealkylation with pentyl chain loss ($-C_5H_{10}$) led to A4 formation. Major fragments were produced by carboxamide (*m/z* 230.1285) and aminodimethylbutanamide (*m/z* 145.0395) loss. This reaction is common for SC with an *N*-pentyl chain *(25, 26)* with a low/intermediate signal intensity, although it was not reported in AB-PINACA metabolism *(23)*. A4 also was reported in ADB-FUBINACA metabolism after methylenefluorophenyl loss with a low intensity *(29)*.

ADB-PINACA DIHYDRODIOL FORMATION

Epoxidation (+O) of a double bond followed by hydrolysis ($+H_2O$) to the corresponding *trans*-dihydrodiol is a common mechanism in mammals' metabolism *(33)*, as previously reported in synthetic cannabinoids with an indole or indazole core *(23, 27, 29)*. A7 presented a +34.0057-Da mass shift from parent. All fragments included the same mass shift, including fragment *m/z* 179.0449 (*m/z* 145.0394 +O $+H_2O$), indicating a dihydrodiol formation at the indazole ring.

5F-ADB-PINACA METABOLITES IN HUMAN HEPATOCYTES

In contrast to ADB-PINACA, 5F-ADB-PINACA was almost completely metabolized after 3 h incubation. Thirty-two different metabolites were identified, with 12 yielding >95% of the metabolites' total peak area (F1–F12 in ascending retention time order, Fig. 5). Oxidative defluorination (F1, F3, F7, F11; F6 as glucuronide) and subsequent carboxylation (F5, F9, F10, F12) were the 2 principle metabolic reactions, in accordance with other *N*-5-fluoropentyl SC *(23–25, 28, 34)*. F7 (ADB-PINACA 5-hydroxypentyl) and F9 (ADB-PINACA pentanoic acid) yielded 74.8% of the metabolites' total peak area. Contrary to ADB-PINACA metabolism, pentyl hydroxylation (F1, F8) was secondary. Other minor phase I reactions included isopropyl hydroxylation (F3, F5), *N*-depentylation (F4), oxidative deamination of the carboxamide group (F10-F12), and isopropyl dehydrogenation (F11, F12). Two metabolites (F2, F6) underwent phase II glucuronidation. Results are compiled in Table 1. MS/MS spectra and fragmentation patterns are depicted in Fig. 3, with the data for 8 minor metabolites provided in the online Supplemental Figs. 4 and 5. A proposed metabolic pathway for 5F-ADB-PINACA is described in Fig. 5.

5F-ADB-PINACA OXIDATION AND FURTHER GLUCURONIDATION

F8 was hydroxylated at the pentyl chain, as indicated by the +15.9944-Da mass difference from parent and the detection of indazole fragments, *m/z* 145.0395 and 177.0459, along with hydroxylated fragments with dimethylbutanamide (*m/z* 267.1136) and aminodimethylbutanamide (*m/z* 249.1030) loss.

F2 mass shift of +192.0268 Da from parent was consistent with an oxidation (+O) followed by glucuronidation ($+C_6H_8O_6$). Like A6, the corresponding ADB-PINACA metabolite, F2's MS/MS spectrum displayed fragment *m/z* 161.0343 produced by the hydroxylated indazole moiety (*m/z* 145.0394 +O), pointing toward a hydroxy-glucuronidation at the indazole ring. Fragments *m/z* 443.1455 and 425.1344, respectively produced by dimethylbutanamide and aminodimethylbutanamide loss, and their subsequent glucuronide loss, *m/z* 267.1136 and 249.1029, further confirmed hydroxy-glucuronidation.

5F-ADB-PINACA OXIDATIVE DEFLUORINATION AND FURTHER METABOLISM

F7 was the result of 5F-ADB-PINACA oxidative defluorination (−F +OH), as suggested by the −1.9959-Da mass decrease from parent. Fragmentation produced the same ions observed with other ADB-PINACA hydroxypentyl metabolites, confirming oxidative defluorination. Numerous secondary metabolites were generated from F7, including F7 glucuronidation that produced F6.

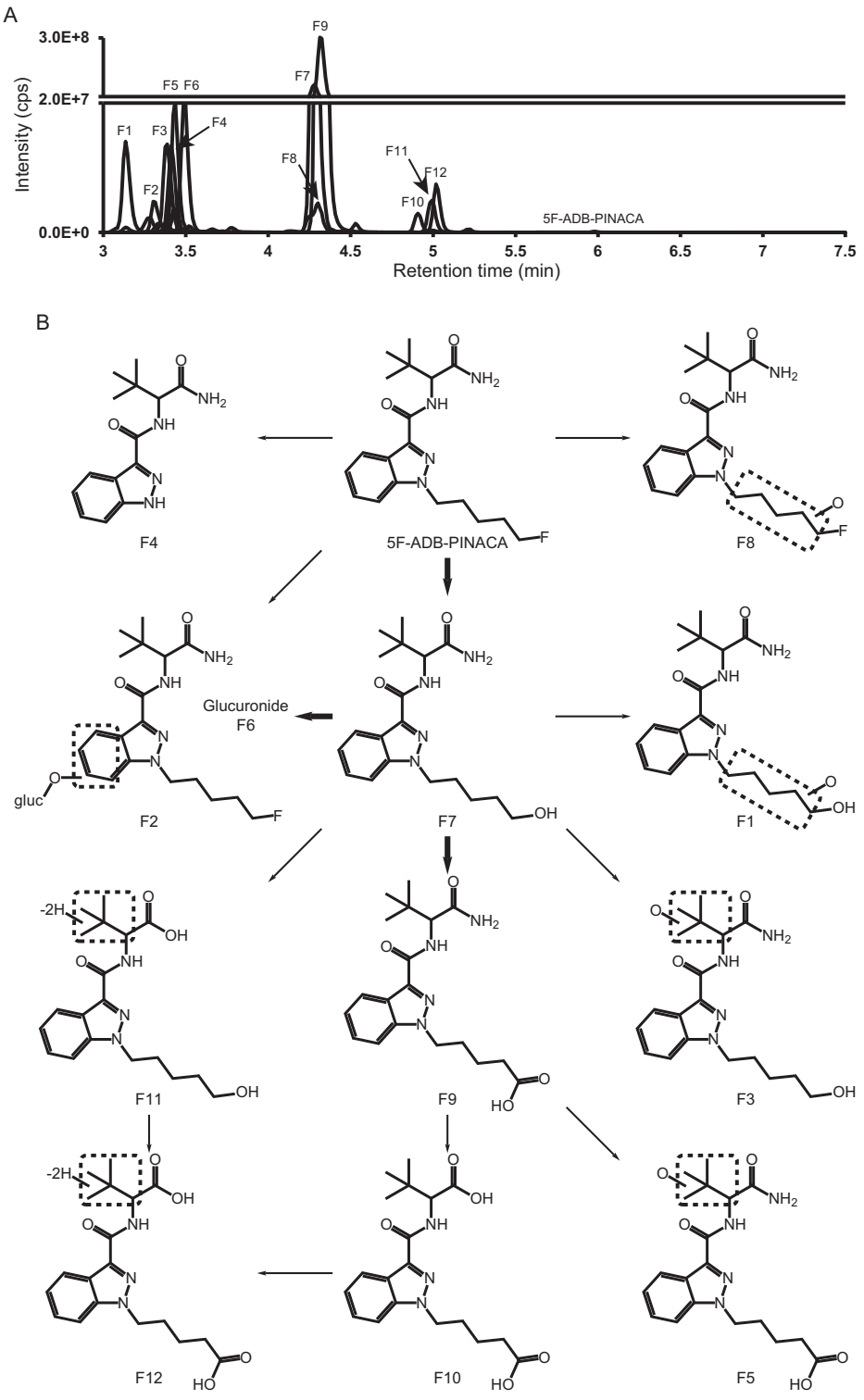

Fig. 5. Combined extracted ion chromatogram (A) and proposed metabolic pathway (B) of 5F-ADB-PINACA and metabolites obtained from 3-h hepatocyte incubation.

Bold arrow, major pathway; gluc, glucuronide.

Minor metabolite F1 combined oxidative defluorination and pentyl hydroxylation, as described above. F3 combined oxidative defluorination and isopropyl hydroxylation, as indicated by the +15.9950-Da mass shift from F7 (+13.9991 Da from parent). The mass deviation was transferred to fragments produced by amine (*m/z* 360.1910) and carboxamide (*m/z* 332.1959) loss. As described for A17 that carried the same hydroxyisopropyl group, carboxamide loss was mostly followed by hydroxymethyl loss (*m/z* 302.1857).

F9 was produced by further F7 oxidation to pentanoic acid formation, as indicated by the +15.9948 −2.0156-Da mass shift from F9. It was the metabolite with the most intense signal in 5F-ADB-PINACA incubation, yielding 61.3% of the metabolites' total peak area. F5 was produced by further isopropyl hydroxylation as described above. The compound was fragmented along with a common phthalate at *m/z* 391.2838 ($C_{24}H_{38}O_4$) *(34)* that generated contaminants at *m/z* 57.0701, 71.0855, 149.0232, and 167.0338. The plasticizer was released by LC tubing and was present in the mobile phase throughout the entire chromatographic separation (signal was 27.6% F5 at F5 retention time).

F10, F11, and F12 were minor third and fourth generation metabolites combining oxidative defluorination and subsequent carboxylation and oxidative deamination (F10), oxidative defluorination, oxidative deamination, and isopropyl dehydrogenation (F11) and oxidative defluorination and subsequent carboxylation, oxidative deamination, and isopropyl dehydrogenation (F12).

5F-ADB-PINACA *N*-DEPENTYLATION

F4 was produced by 5F-ADB-PINACA *N*-defluoropentylation ($-C_5H_9F$). The metabolite is shared with ADB-PINACA (A4) and ADB-FUBINACA *(29)* metabolism. This is a common, although minor, reaction for SC with an *N*-5-fluoropentyl chain *(25, 28)*.

TARGETS FOR ADB-PINACA AND 5F-ADB-PINACA INTAKE

ADB-PINACA and 5F-ADB-PINACA displayed a similar pattern of major metabolites as JWH-018/AM-2201 *(35)*, THJ-018/THJ-2201 *(25)*, and other SC 5-fluoro analogs *(23)*. Both mainly generated ADB-PINACA hydroxypentyl metabolites and derivatives. However, the site of attack was different between the 2, resulting in different major metabolites. 5F-ADB-PINACA metabolites mainly resulted from oxidative defluorination and subsequent carboxylation, leading to the formation of ADB-PINACA 5-hydroxypentyl, ADB-PINACA pentanoic acid, and derivatives. In contrast, ADB-PINACA 5-hydroxypentyl and pentanoic acid were minor in ADB-PINACA metabolism, in which hydroxylation at C_1–C_4 and subsequent ketone formation mainly occurred. Therefore, we propose ADB-PINACA 5-hydroxypentyl (F7) and ADB-PINACA pentanoic acid (F9) as targets for 5F-ADB-PINACA intake, and ADB-PINACA ketopentyl (A12) and ADB-PINACA hydroxypentyl (A9 and A11) as targets for ADB-PINACA intake. None of these compounds was reported as a metabolite from another SC. It is noteworthy that A9, F7, and A11 are positional isomers with close retention time (4.18, 4.28, and 4.44 min, respectively). However, although they produce the same fragments in MS/MS, the relative intensities of fragments *m/z* 213.1019, 231.1124, and 249.1230 are different. A pertinent choice of MS/MS transitions and an optimized chromatographic gradient are required for a clear differentiation.

To increase detection capability of nonconjugated metabolites, most of the screening methods for SC in urine target only phase I metabolites after sample hydrolysis *(22, 36, 37)*. Phase II glucuronidation plays a minor role in ADB-PINACA and 5F-ADB-PINACA metabolism. However, major metabolites A9 and F7 concentrations may increase after A3 and F6 hydrolysis, improving their detection. In addition, instability of glucuronidated cannabinoids at room temperature was previously reported *(38)*. Accordingly, we recommend systematic hydrolysis of urinary samples following ADB-PINACA or 5F-ADB-PINACA intake.

Conclusions

Identification of major markers for distinguishing ADB-PINACA and 5F-ADB-PINACA intake is critical for toxicological and legal purposes. We identified 19 and 12 major metabolites after 3-h incubation of ADB-PINACA and 5F-ADB-PINACA, respectively, with human hepatocytes. We recommend ADB-PINACA ketopentyl (A12) and hydroxypentyl (A9 and A11) to identify ADB-PINACA intake, and ADB-PINACA 5-hydroxypentyl (F7) and pentanoic acid (F9) to identify 5F-ADB-PINACA intake. Analysis of urine samples from authentic ADB-PINACA and 5F-ADB-PINACA intake cases would have been useful to confirm results, since human hepatocytes cannot reproduce extrahepatic metabolism. Unfortunately, despite our efforts, we could not obtain such samples. However, as observed with structural analogs AB-FUBINACA *(27)*, AB-PINACA, and 5F-AB-PINACA *(23)*, in vitro human hepatocyte metabolite profiles proved to match well with those of authentic urine samples. Identifying these metabolites should help manufacturers focus their efforts on the synthesis of suitable analytical standards that will allow metabolite quantification and further pharmacodynamic and pharmacokinetic studies.

Author Contributions: *All authors confirmed they have contributed to the intellectual content of this paper and have met the following 3 requirements: (a) significant contributions to the conception and design, acquisition of*

data, or analysis and interpretation of data; (b) drafting or revising the article for intellectual content; and (c) final approval of the published article.

Authors' Disclosures or Potential Conflicts of Interest: *Upon manuscript submission, all authors completed the author disclosure form. Disclosures and/or potential conflicts of interest:*

Employment or Leadership: None declared.
Consultant or Advisory Role: None declared.
Stock Ownership: None declared.
Honoraria: None declared.
Research Funding: The Intramural Research Program of the National Institute on Drug Abuse, NIH.

Expert Testimony: None declared.
Patents: None declared.

Role of Sponsor: The funding organizations played no role in the design of study, choice of enrolled patients, review and interpretation of data, and final approval of manuscript.

Acknowledgments: The authors thank Tim Moeller from BioreclamationIVT for his assistance with the incubations, and Caroline Ding, Helen Sun, and Thermo Scientific for providing LC-HRMS instrumentation, Compound Discoverer® software and training via a collaboration agreement.

References

1. Gurney SM, Scott KS, Kacinko SL, Presley BC, Logan BK. Pharmacology, toxicology, and adverse effects of synthetic cannabinoid drugs. Forensic Sci Rev 2014;26: 53–78.
2. Auwarter V, Dresen S, Weinmann W, Muller M, Putz M, Ferreiros N. "Spice" and other herbal blends: harmless incense or cannabinoid designer drugs? J Mass Spectrom 2009;44:832–7.
3. Labay LM, Caruso JL, Gilson TP, Phipps RJ, Knight LD, Lemos NP, et al. Synthetic cannabinoid drug use as a cause or contributory cause of death. Forensic Sci Int 2016;260:31–9.
4. Kamijo Y, Takai M, Fujita Y, Sakamoto T. A multicenter retrospective survey of poisoning after consumption of products containing novel psychoactive substances from 2013 to 2014 in Japan. Am J Drug Alcohol Abuse 2016;42:513–9.
5. European Monitoring Centre for Drugs and Drug Addiction. European drug report: trends and developments. 2016. http://www.emcdda.europa.eu/system/files/publications/2637/TDAT16001ENN.pdf (Accessed January 2017).
6. Weatherholt TJ. Not for human consumption: how inept legislative policy proliferates the synthetic drug problem. 2015. http://www.kentuckylawjournal.org/index.php/2015/02/22/not-for-human-consumption/ (Accessed January 2017).
7. Drugs-Forum. Research chemicals - cannabinoids. https://drugs-forum.com/forum/forumdisplay.php?f=336 (Accessed January 2017).
8. Banister SD, Moir M, Stuart J, Kevin RC, Wood KE, Longworth M, et al. Pharmacology of indole and indazole synthetic cannabinoid designer drugs AB-FUBINACA, ADB-FUBINACA, AB-PINACA, ADB-PINACA, 5F-AB-PINACA, 5F-ADB-PINACA, ADBICA, and 5F-ADBICA. ACS Chem Neurosci 2015;6:1546–59.
9. Monte AA, Bronstein AC, Cao DJ, Heard KJ, Hoppe JA, Hoyte CO, et al. An outbreak of exposure to a novel synthetic cannabinoid. N Engl J Med 2014;370:389–90.
10. Schwartz MD, Trecki J, Edison LA, Steck AR, Arnold JK, Gerona RR. A common source outbreak of severe delirium associated with exposure to the novel synthetic cannabinoid ADB-PINACA. J Emerg Med 2015;48: 573–80.
11. European Monitoring Centre for Drugs and Drug Addiction. EMCDDA-Europol 2013 annual report on the implementation of Council Decision 2005/387/JHA. Implementation reports. Lisbon: EMCDDA-Europol; 2014.
12. European Monitoring Centre for Drugs and Drug Addiction. EMCDDA-Europol 2014 annual report on the implementation of Council Decision 2005/387/JHA. Implementation reports 2015. : EMCDDA-Europol; 2015.
13. Wurita A, Hasegawa K, Minakata K, Gonmori K, Nozawa H, Yamagishi I, et al. Identification and quantitation of 5-fluoro-ADB-PINACA and MAB-CHMINACA in dubious herbal products. Forensic Toxicol 2015;33:213–20.
14. European Monitoring Centre for Drugs and Drug Addiction. EMCDDA-Europol 2015 annual report on the implementation of Council Decision 2005/387/JHA. Implementation reports 2016. Lisbon: EMCDDA-Europol; 2016.
15. Department of Justice, Drug Enforcement Administration. Schedules of controlled substances: temporary placement of four synthetic cannabinoids into schedule I. Fed Regist 2014;79:7577–82.
16. Department of Justice, Drug Enforcement Administration. Schedules of controlled substances: extension of temporary placement of PB-22, 5F-PB-22, AB-FUBINACA and ADB-PINACA in schedule I of the controlled substances act. Fed Regist 2016;81:6175–7.
17. China Food and Drug Administration. Notice on issuing the measures for the administration of non - medicinal narcotic drugs and psychotropic drugs: public words [2015] on the 27th [in Chinese]. 2015. http://www.sfda.gov.cn/WS01/CL0056/130753.html (Accessed January 2017).
18. National Institute of Health Sciences. Data Search System for New Psychoactive Substances. http://npsdb.nihs.go.jp/Search/Search/AllCompounds_e.aspx (Accessed August 2016).
19. Central Narcotics Bureau. Misuse of drugs act. CNB news release 2015. www.cnb.gov.sg/Libraries/CNB_Newsroom_Files/CNB_NR_-_30_Apr_2015.sflb.ashx (Accessed January 2017).
20. Bertol E, Vaiano F, Di Milia MG, Mari F. In vivo detection of the new psychoactive substance AM-694 and its metabolites. Forensic Sci Int 2015;256:21–7.
21. Jang M, Kim IS, Park YN, Kim J, Han I, Baeck S, et al. Determination of urinary metabolites of XLR-11 by liquid chromatography-quadrupole time-of-flight mass spectrometry. Anal Bioanal Chem 2016;408:503–16.
22. Franz F, Angerer V, Moosmann B, Auwarter V. Phase I metabolism of the highly potent synthetic cannabinoid MDMB-CHMICA and detection in human urine samples. Drug Test Anal [Epub ahead of print 2016 Aug 9].
23. Wohlfarth A, Castaneto MS, Zhu M, Pang S, Scheidweiler KB, Kronstrand R, Huestis MA. Pentylindole/pentylindazole synthetic cannabinoids and their 5-fluoro analogs produce different primary metabolites: metabolite profiling for AB-PINACA and 5F-AB-PINACA. AAPS J 2015;17:660–77.
24. Andersson M, Diao X, Wohlfarth A, Scheidweiler KB, Huestis MA. Metabolic profiling of new synthetic cannabinoids AMB and 5F-AMB by human hepatocyte and liver microsome incubations and high-resolution mass spectrometry. Rapid Commun Mass Spectrom 2016; 30:1067–78.
25. Diao X, Wohlfarth A, Pang S, Scheidweiler KB, Huestis MA. High-resolution mass spectrometry for characterizing the metabolism of synthetic cannabinoid THJ-018 and its 5-fluoro analog THJ-2201 after incubation in human hepatocytes. Clin Chem 2016;62:157–69.
26. Gandhi AS, Zhu M, Pang S, Wohlfarth A, Scheidweiler KB, Huestis MA. Metabolite profiling of RCS-4, a novel synthetic cannabinoid designer drug, using human hepatocyte metabolism and TOF-MS. Bioanalysis 2014;6: 1471–85.
27. Castaneto M, Wohlfarth A, Pang S, Zhu M, Scheidweiler KB, Kronstrand R, Huestis MA. Identification of AB-FUBINACA metabolites in human hepatocytes and urine using high-resolution mass spectrometry. Forensic Toxicol 2015;33:295–310.
28. Diao X, Scheidweiler KB, Wohlfarth A, Zhu M, Pang S, Huestis MA. Strategies to distinguish new synthetic cannabinoid FUBIMINA (BIM-2201) intake from its isomer THJ-2201: metabolism of FUBIMINA in human hepatocytes. Forensic Toxicol 2016;34:256–67.
29. Carlier J, Diao X, Wohlfarth A, Scheidweiler KB, Huestis MA. In vitro metabolic profiling of ADB-FUBINACA, a new synthetic cannabinoid. Curr Neuropharmacol [Epub ahead of print 2016 Nov 8].
30. Li AP. Human hepatocytes: isolation, cryopreservation and applications in drug development. Chem Biol Interact 2007;168:16–29.
31. Sohlenius-Sternbeck AK, Chelpin HV, Orzechowski A, Halldin MM. Metabolism of sameridine to monocarboxylated products by hepatocytes isolated from the male rat. Drug Metab Dispos 2000;28:695–700.
32. Diao X, Deng P, Xie C, Li X, Zhong D, Zhang Y, Chen X. Metabolism and pharmacokinetics of 3-n-butylphthalide (NBP) in humans: the role of cytochrome P450s and alcohol dehydrogenase in biotransformation. Drug Metab Dispos 2013;41:430–44.
33. Hsia MT. Toxicological significance of dihydrodiol metabolites. J Toxicol Clin Toxicol 1982;19:737–58.
34. Weber RJ, Li E, Bruty J, He S, Viant MR. Maconda: a publicly accessible mass spectrometry contaminants database. Bioinformatics 2012;28:2856–7.
35. Hutter M, Moosmann B, Kneisel S, Auwarter V. Characteristics of the designer drug and synthetic cannabinoid receptor agonist AM-2201 regarding its chemistry and metabolism. J Mass Spectrom 2013;48:885–94.
36. Scheidweiler KB, Jarvis MJ, Huestis MA. Nontargeted swath acquisition for identifying 47 synthetic cannabinoid metabolites in human urine by liquid chromatography-high-resolution tandem mass spectrometry. Anal Bioanal Chem 2015;407:883–97.
37. Neifeld JR, Regester LE, Holler JM, Vorce SP, Magluilo J, Jr., Ramos G, Bosy TZ. Ultrafast screening of synthetic cannabinoids and synthetic cathinones in urine by rapidfire-tandem mass spectrometry. J Anal Toxicol

2016;40:379–87.
38. Scheidweiler KB, Schwope DM, Karschner EL, Desrosiers NA, Gorelick DA, Huestis MA. In vitro stability of free and glucuronidated cannabinoids in blood and plasma following controlled smoked cannabis. Clin Chem 2013;59:1108–17.
39. Caspar AT, Helfer AG, Michely JA, Auwarter V, Brandt SD, Meyer MR, Maurer HH. Studies on the metabolism and toxicological detection of the new psychoactive designer drug 2-(4-iodo-2,5-dimethoxyphenyl)-n-[(2-methoxyphenyl)methyl]ethanamine (25I-NBOMe) in human and rat urine using GC-MS, LC-MS(n), and LC-HR-MS/MS. Anal Bioanal Chem 2015;407:6697–719.
40. Schaefer N, Helfer AG, Kettner M, Laschke MW, Schlote J, Ewald AH, et al. Metabolic patterns of JWH-210, RCS-4, and THC in pig urine elucidated using LC-HR-MS/MS: do they reflect patterns in humans? Drug Test Anal [Epub ahead of print 2016 Jun 22].